THREE-DIMENSIONAL ANALYSIS OF MICROSCOPIC STRESS DISTRIBUTION AT A FREE EDGE OF A CROSS-PLY CFRP LAMINATE

K. Goto[1], T. Matsuda[1]*
[1] Department of Engineering Mechanics and Energy, University of Tsukuba, Tsukuba, Japan
* Corresponding author (matsuda@kz.tsukuba.ac.jp)

Keywords: *CFRP laminate, Free edge, Microscopic stress, Interlaminar, Homogenization*

1 Introduction

Carbon fiber-reinforced plastic laminates (CFRP laminates) are now regarded as some of the most important engineering materials, because of their excellent specific strength and specific stiffness. These properties contribute to the weight reduction of high-end engineering products such as aircraft, spacecraft and automobiles. This leads to a significant improvement in energy efficiency, resulting in the reduction of environmental load.

In general, CFRP laminates have extremely heterogeneous microscopic structures compared to conventional metallic materials. This is because they are manufactured by stacking unidirectional reinforced laminae called pre-preg sheets comprised of a polymer matrix and unidirectionally aligned carbon fibers. This can cause complex distribution of microscopic stress and, in some cases, high stress concentration in laminates. Therefore, such microscopic stress distribution in laminates has to be taken into account during the mechanical design and estimation of CFRP laminates. In particular, it is of great importance to examine the stress distribution at the free edges of laminates, where high shear stress concentration is apt to occur. Such stress concentration generally takes place at the lamina/lamina interfaces (interlaminar) and the fiber/matrix interfaces [1] around the free edges due to the mismatch of deformation resulting from the difference of their material constants. This is sometimes called the "edge-effect", and can bring about microscopic failures of the laminates, which may result in the macroscopic fracture of the laminates themselves. It is therefore necessary to investigate the microscopic stress distribution at the free edges of CFRP laminates.

The mathematical homogenization theory for periodic materials [2] is one of the most useful theories for analyzing mechanical behavior of composites such as CFRP laminates, because this theory can analyze both the macroscopic behavior of the composites and the microscopic stress distribution in them at the same time. Thus, in the previous studies, the present authors developed the homogenization theory applicable to non-linear time-dependent problems [3], and analyzed the elastic-viscoplastic and creep behaviors of CFRP laminates using the developed theory [4,5]. Moreover, the present authors [6] also analyzed interlaminar stress distribution in cross-ply CFRP laminates using the homogenization theory. Through these analyses, the authors have found high applicability of the homogenization theory to various mechanical problems of CFRP laminates. These analyses, however, were not able to deal with the free edges of laminates, because all of them were based on the homogenization theory which was applicable only to infinite periodic materials. On the other hand, there have been reports on some studies which have analyzed the microscopic stress at the edges of FRPs using the finite element method (FEM) [7,8]. However, these analyses were limited to two-dimensional problems of unidirectional FRPs subjected to a transverse loading. In this situation, the edge effect mentioned before does not occur, resulting in an insufficient understanding of the edge problems of CFRP laminates.

In this study, the microscopic stress distribution at a free edge of a cross-ply CFRP laminate is analyzed three-dimensionally based on the homogenization theory. First, by considering a CFRP laminate with free edges and defining its unit cell, the homogenization theory is reconstructed so that it can

be applied to the edge problem of the laminate. Then, the unit cell is reduced by half using point-symmetry of the internal structure of the laminate. Moreover, the substructure method [9] is introduced into the present method for reduction of computational costs. Using the proposed method, the microscopic stress distribution and stress concentration at a edge of a cross-ply carbon fiber/epoxy laminate are examined.

2 Theory

2.1 Cross-ply CFRP Model

Consider a cross-ply CFRP laminate subjected to a macroscopic uniaxial load in the y_2 - y_3 plane (Fig. 1). This laminate is reinforced in the y_1 - and y_3 -directions, and has a finite length in the y_1 -direction, i.e. it has the free edges as illustrated in Fig. 1. On the other hand, the laminate is assumed to be infinite in the y_2 - and y_3 -directions. The carbon fibers in each ply are arranged squarely in the plane perpendicular to them for simplicity.

2.2 Homogenization Theory with Free Edges

For the above-mentioned laminate, a unit cell Y has been defined as indicated in Fig. 1. Describing the microscopic distributions of stress and strain in Y as $\sigma_{ij}(\boldsymbol{y})$ and $\varepsilon_{ij}(\boldsymbol{y})$, respectively, the equilibrium of σ_{ij} can be expressed as

$$\sigma_{ij,j} = 0, \tag{1}$$

where $(\ )_{,j}$ denotes the differentiation with respect to y_j. The fibers and matrix in the laminate are assumed to exhibit linear elasticity as characterized

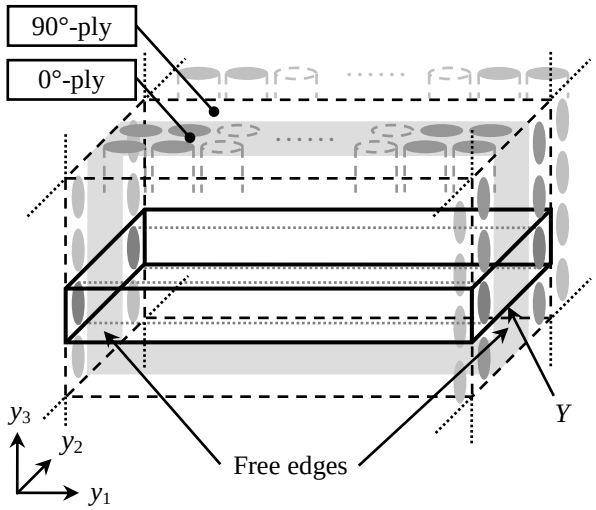

Fig. 1. Cross-ply CFRP laminates and unit cell *Y*.

by

$$\sigma_{ij} = c_{ijkl}\varepsilon_{kl}, \tag{2}$$

where c_{ijkl} indicates the elastic stiffness of the fibers and matrix. The microscopic displacement field $u_i(\boldsymbol{y})$ in Y has the following expression:

$$u_i(\boldsymbol{y}) = u_i^0(\boldsymbol{y}) + u_i^{\#}(\boldsymbol{y}), \tag{3}$$

where u_i^0 and $u_i^{\#}$ denote the macroscopic displacement and the perturbed displacement, respectively. Then the microscopic strain ε_{ij} in Eq. (2) is expressed as a sum of the macroscopic strain E_{ij} and the perturbed strain $\varepsilon_{ij}^{\#}$, i.e.

$$\varepsilon_{ij} = E_{ij} + \varepsilon_{ij}^{\#}. \tag{4}$$

Let $\delta u_i^{\#}$ be an arbitrary variation of the perturbed displacement field defined in Y. Then, the integration by parts and the divergence theorem allow Eq. (1) to be transformed to

$$\int_Y \sigma_{ij}\delta u_{i,j}^{\#} dY - \int_\Gamma \sigma_{ij} n_j \delta u_i^{\#} d\Gamma = 0, \tag{5}$$

where Γ denotes the boundary of Y, and n_i indicates the unit vector outward normal to Γ. In the above equation, the second term of the left-hand side, i.e. the boundary integral term, vanishes because of the following reasons: First, on the top and bottom, and front and rear boundary facets of Y, σ_{ij} and $\delta u_i^{\#}$ distribute Y -periodically, while n_i takes a opposite direction on a opposite boundary facet. Thus, the boundary integral term in Eq. (5) becomes zero on these boundary facets. This is the same situation as in the usual homogenization theory which deals with infinite periodic materials. In contrast, on the left and right boundary facets, the above situation holds as it is with respect to the y_2 - and y_3 -directions, whereas it does not hold in the y_1 -direction because the Y -periodicity in this direction no longer exists. However, regarding the y_1 -direction, σ_{ij} is zero because the left and right boundary facets are the free edges. The boundary integral term on these facets, therefore, also becomes zero. Consequently, the second term of the left-hand side in Eq. (5) vanishes, resulting in

$$\int_Y \sigma_{ij}\delta u_{i,j}^{\#} dY = 0. \tag{6}$$

This resulting equation has the same form as that obtained from the conventional homogenization theory. Thus, the field of microscopic stress σ_{ij} in Y and the relation between macroscopic stress Σ_{ij}

and macroscopic strain E_{ij} of the laminate are derived in the same forms as in the conventional homogenization theory: [2]

$$\sigma_{ij} = c_{ijpq}(\delta_{pk}\delta_{ql} + \chi^{kl}_{p,q})E_{kl}\,, \tag{7}$$

$$\Sigma_{ij} = \left\langle c_{ijpq}(\delta_{pk}\delta_{ql} + \chi^{kl}_{p,q})\right\rangle E_{kl}\,, \tag{8}$$

where δ_{ij} indicates Kronecker's delta, and $\langle\ \rangle$ designates the volume average in Y defined as $\langle \# \rangle = |Y|^{-1}\int_Y \# dY$, in which $|Y|$ signifies the volume of Y. Moreover, χ^{kl}_i in Eqs. (7) and (8) denotes the characteristic function determined by solving the following boundary value problem:

$$\int_Y c_{ijpq}\chi^{kl}_{p,q}\delta u^{\#}_{i,j}dY = -\int_Y c_{ijkl}\delta u^{\#}_{i,j}dY\,. \tag{9}$$

It should be noted that, when solving the above problem, the traction-free boundary condition with respect to the y_1-direction on the left and right boundary facets, and the Y-periodic boundary condition with respect to the others are imposed on χ^{kl}_i.

2.3 Semiunit Cell

Consider half of the unit cell Y as illustrated in Fig. 2, which hereafter is referred to as a semiunit cell $\tilde{Y}$. A close look at Fig. 2 reveals that the internal structure of the laminate has a point-symmetry with respect to the center of the left boundary facet of $\tilde{Y}$, C. Consequently, the distribution of χ^{kl}_i also satisfies the point-symmetry with respect to this point. Using the point-symmetry as a boundary condition on the left boundary facet, $\tilde{Y}$ instead of Y can be employed as the domain of analysis, leading to the following boundary value problem with respect to $\tilde{Y}$: [10]

$$\int_{\tilde{Y}} c_{ijpq}\chi^{kl}_{p,q}\delta u^{\#}_{i,j}d\tilde{Y} = -\int_{\tilde{Y}} c_{ijkl}\delta u^{\#}_{i,j}d\tilde{Y}\,. \tag{10}$$

When solving Eq. (10), the point-symmetric boundary condition with respect to C on the left boundary facet is imposed on χ^{kl}_i.

2.4 Substructure Method

First, the semiunit cell $\tilde{Y}$ is divided into cubic substructures A_i and B_i ($i = 1, 2, ..., N$) as shown in Fig. 3 (in this figure, N is set to be 16 (8 x 4 substructures) in accordance with the analysis in the next section). Then the boundary value problems for the individual substructures in a finite element discretized form are derived as follows: [6,9]

$$\boldsymbol{K}_A\boldsymbol{\chi}^{kl}_{A_i} = \boldsymbol{F}^{kl}_A\,,\ (i = 1, 2, ..., N)\,, \tag{11}$$

$$\boldsymbol{K}_B\boldsymbol{\chi}^{kl}_{B_i} = \boldsymbol{F}^{kl}_B\,,\ (i = 1, 2, ..., N)\,, \tag{12}$$

where $\boldsymbol{\chi}^{kl}_{A_i}$ and $\boldsymbol{\chi}^{kl}_{B_i}$ denote the nodal vectors of characteristic function in A_i and B_i, respectively, and $\boldsymbol{K}_A$, $\boldsymbol{F}^{kl}_A$, $\boldsymbol{K}_B$, and $\boldsymbol{F}^{kl}_B$ have the following expressions:

$$\boldsymbol{K}_A = \int_{A_i}\boldsymbol{B}^{\mathrm{T}}\boldsymbol{C}\boldsymbol{B}dA_i\,,\ \boldsymbol{F}^{kl}_A = -\int_{A_i}\boldsymbol{B}^{\mathrm{T}}\boldsymbol{C}^{kl}dA_i\,, \tag{13}$$

$$\boldsymbol{K}_B = \int_{B_i}\boldsymbol{B}^{\mathrm{T}}\boldsymbol{C}\boldsymbol{B}dB_i\,,\ \boldsymbol{F}^{kl}_B = -\int_{B_i}\boldsymbol{B}^{\mathrm{T}}\boldsymbol{C}^{kl}dB_i\,, \tag{14}$$

It is noteworthy that all A_i have common $\boldsymbol{K}_A$ and $\boldsymbol{F}^{kl}_A$ because the geometry and material properties of all A_i are the same. For the same reason, all B_i

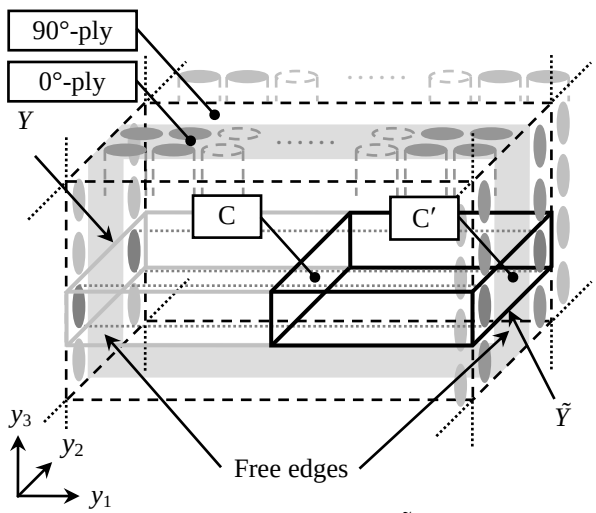

Fig. 2. Semiunit cell $\tilde{Y}$.

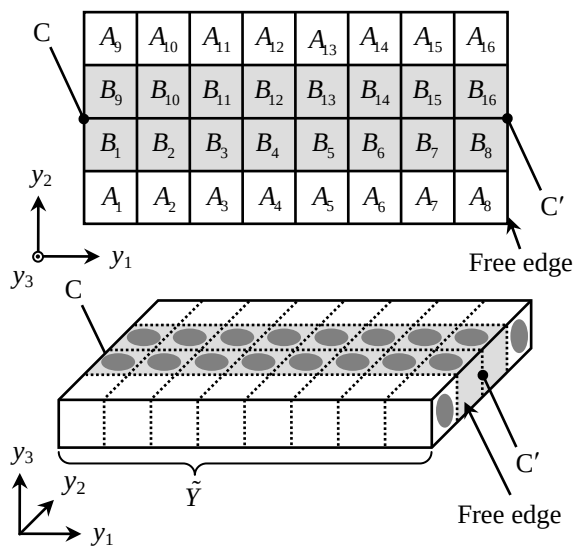

Fig. 3. Semiunit cell $\tilde{Y}$ and substructures.

have common $\boldsymbol{K}_B$ and $\boldsymbol{F}_B^{kl}$, which are easily obtained by rotating A_i by 90° with respect to the y_2-direction. It is therefore enough for us to calculate $\boldsymbol{K}_A$, $\boldsymbol{F}_A^{kl}$, $\boldsymbol{K}_B$, and $\boldsymbol{F}_B^{kl}$ only once.

Next, the components of $\boldsymbol{\chi}_{A_i}^{kl}$ are divided into two parts, $\boldsymbol{\chi}_{A_i}^{kl(\Omega)}$ and $\boldsymbol{\chi}_{A_i}^{kl(\Gamma)}$, which represent the characteristic functions at the internal and the boundary nodes of A_i, respectively. The components of $\boldsymbol{\chi}_{B_i}^{kl}$ are also divided into $\boldsymbol{\chi}_{B_i}^{kl(\Omega)}$ and $\boldsymbol{\chi}_{B_i}^{kl(\Gamma)}$. Then, the boundary value problems for A_i and B_i, Eqs. (11) and (12), are rewritten into the following equations, respectively:

$$\begin{bmatrix} \boldsymbol{K}_A^{(\Omega)} & \boldsymbol{K}_A^{(\Omega\Gamma)} \\ \boldsymbol{K}_A^{(\Gamma\Omega)} & \boldsymbol{K}_A^{(\Gamma)} \end{bmatrix} \begin{Bmatrix} \boldsymbol{\chi}_{A_i}^{kl(\Omega)} \\ \boldsymbol{\chi}_{A_i}^{kl(\Gamma)} \end{Bmatrix} = \begin{Bmatrix} \boldsymbol{F}_A^{kl(\Omega)} \\ \boldsymbol{F}_A^{kl(\Gamma)} \end{Bmatrix}, \tag{15}$$

$$\begin{bmatrix} \boldsymbol{K}_B^{(\Omega)} & \boldsymbol{K}_B^{(\Omega\Gamma)} \\ \boldsymbol{K}_B^{(\Gamma\Omega)} & \boldsymbol{K}_B^{(\Gamma)} \end{bmatrix} \begin{Bmatrix} \boldsymbol{\chi}_{B_i}^{kl(\Omega)} \\ \boldsymbol{\chi}_{B_i}^{kl(\Gamma)} \end{Bmatrix} = \begin{Bmatrix} \boldsymbol{F}_B^{kl(\Omega)} \\ \boldsymbol{F}_B^{kl(\Gamma)} \end{Bmatrix}, \tag{16}$$

and we obtain

$$\boldsymbol{\chi}_{A_i}^{kl(\Omega)} = \left(\boldsymbol{K}_A^{(\Omega)}\right)^{-1}\left(\boldsymbol{F}_A^{kl(\Omega)} - \boldsymbol{K}_A^{(\Omega\Gamma)}\boldsymbol{\chi}_{A_i}^{kl(\Gamma)}\right), \tag{17}$$

$$\boldsymbol{\chi}_{B_i}^{kl(\Omega)} = \left(\boldsymbol{K}_B^{(\Omega)}\right)^{-1}\left(\boldsymbol{F}_B^{kl(\Omega)} - \boldsymbol{K}_B^{(\Omega\Gamma)}\boldsymbol{\chi}_{B_i}^{kl(\Gamma)}\right). \tag{18}$$

The elimination of $\boldsymbol{\chi}_{A_i}^{kl(\Omega)}$ and $\boldsymbol{\chi}_{B_i}^{kl(\Omega)}$ from Eqs. (15) and (16) using the above equations, respectively, yields

$$\bar{\boldsymbol{K}}_A^{(\Gamma)}\boldsymbol{\chi}_{A_i}^{kl(\Gamma)} = \bar{\boldsymbol{F}}_A^{kl(\Gamma)}, \tag{19}$$

$$\bar{\boldsymbol{K}}_B^{(\Gamma)}\boldsymbol{\chi}_{B_i}^{kl(\Gamma)} = \bar{\boldsymbol{F}}_B^{kl(\Gamma)}, \tag{20}$$

where $\bar{\boldsymbol{K}}_A^{(\Gamma)}$, $\bar{\boldsymbol{F}}_A^{kl(\Gamma)}$, $\bar{\boldsymbol{K}}_B^{(\Gamma)}$, and $\bar{\boldsymbol{F}}_B^{kl(\Gamma)}$ are expressed as follows:

$$\begin{aligned} \bar{\boldsymbol{K}}_A^{(\Gamma)} &= \boldsymbol{K}_A^{(\Gamma)} - \boldsymbol{K}_A^{(\Gamma\Omega)}\left(\boldsymbol{K}_A^{(\Omega)}\right)^{-1}\boldsymbol{K}_A^{(\Omega\Gamma)}, \\ \bar{\boldsymbol{F}}_A^{kl(\Gamma)} &= \boldsymbol{F}_A^{kl(\Gamma)} - \boldsymbol{K}_A^{(\Gamma\Omega)}\left(\boldsymbol{K}_A^{(\Omega)}\right)^{-1}\boldsymbol{F}_A^{kl(\Omega)}, \end{aligned} \tag{21}$$

$$\begin{aligned} \bar{\boldsymbol{K}}_B^{(\Gamma)} &= \boldsymbol{K}_B^{(\Gamma)} - \boldsymbol{K}_B^{(\Gamma\Omega)}\left(\boldsymbol{K}_B^{(\Omega)}\right)^{-1}\boldsymbol{K}_B^{(\Omega\Gamma)}, \\ \bar{\boldsymbol{F}}_B^{kl(\Gamma)} &= \boldsymbol{F}_B^{kl(\Gamma)} - \boldsymbol{K}_B^{(\Gamma\Omega)}\left(\boldsymbol{K}_B^{(\Omega)}\right)^{-1}\boldsymbol{F}_B^{kl(\Omega)}. \end{aligned} \tag{22}$$

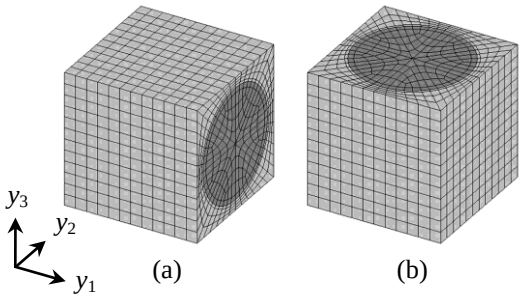

Fig. 4. Substructures (a) A_i and (b) B_i.

Finally, Eqs. (19) and (20) are assembled into one equation, which is a boundary value problem with respect to just the boundary nodes of all substructures, which the joint nodes of adjacent substructures belong to. Thus, we have

$$\boldsymbol{K}^{(\Gamma)}\boldsymbol{\chi}^{kl(\Gamma)} = \boldsymbol{F}^{kl(\Gamma)}, \tag{23}$$

where $\boldsymbol{K}^{(\Gamma)}$ stands for the matrix consisting of $\bar{\boldsymbol{K}}_A^{(\Gamma)}$ and $\bar{\boldsymbol{K}}_B^{(\Gamma)}$, $\boldsymbol{F}^{kl(\Gamma)}$ indicates the vector consisting of $\bar{\boldsymbol{F}}_A^{kl(\Gamma)}$ and $\bar{\boldsymbol{F}}_B^{kl(\Gamma)}$, and $\boldsymbol{\chi}^{kl(\Gamma)}$ denotes the nodal vector of the characteristic function at the boundary nodes of substructures. The characteristic function $\boldsymbol{\chi}^{kl(\Gamma)}$ is determined by solving Eq. (23) with appropriate boundary conditions, i.e., the point-symmetric and the Y-periodic conditions stated in the above subsections, and the continuity condition at the joint nodes of adjacent substructures. Then, the characteristic functions at the internal nodes, $\boldsymbol{\chi}_{A_i}^{kl(\Omega)}$ and $\boldsymbol{\chi}_{B_i}^{kl(\Omega)}$, are calculated using Eqs. (17) and (18).

In general, the total number of boundary nodes of all substructures is much less than the number of all nodes in the domain of analysis, resulting in a significant reduction of computational memory and time.

3 Analysis

3.1 Substructures and Finite Element Discretization

The number of substructures in the semiunit cell $\tilde{Y}$ was set at 8 x 4 along the y_1- and y_2-directions respectively (Fig. 3). Then, each substructure was discretized into eight-node isoparametric elements as depicted in Fig. 4 (4320 elements and 5005 nodes). The volume fraction of fibers was 56%, as in the previous studies [4,5].

3.2 Material Properties

The carbon fibers were regarded as transversely isotropic elastic materials, while the epoxy matrix as an isotropic elastic material. The material constants used in the present analysis are listed in Table 1 [4,5]. In the table, the subscripts L and T indicate the

Table 1 Material constants.

Fiber	$E_{\mathrm{LL}} = 240[\mathrm{GPa}]$	$\nu_{\mathrm{TT}} = 0.49$
	$E_{\mathrm{TT}} = 15.5[\mathrm{GPa}]$	$\nu_{\mathrm{LT}} = 0.28$
	$G_{\mathrm{LT}} = 24.7[\mathrm{GPa}]$	
Epoxy	$E = 3.5[\mathrm{GPa}]$	$\nu = 0.35$

longitudinal and the transverse directions of fibers, respectively.

3.3 Loading Conditions

A uniaxial tensile load in the y_3 -direction was considered, and the macroscopic strain in the loading direction was prescribed to be $E_{33} = 0.5\%$. The present analysis is performed under the macroscopic plane stress condition.

3.4 Results of Analysis

Figs. 5(a)-(c) show the distributions of microscopic resultant shear stress $\tau_{in} = [\tau_{21}{}^2 + \tau_{23}{}^2]^{1/2}$ at the interfaces of A_1-B_1, A_7-B_7 and A_8-B_8, which belong to the interlaminar plane between the 0°- and 90°-plies. On the other hand, Figs. 6(a)-(c) show the distributions of microscopic out-of-plane normal stress σ_{22} at the same interfaces. The deformed shapes of these substructures also depicted in the figures, in which the displacement is magnified 30 times. First, it is seen from Figs. 5(a) and 6(a) that, at the internal area of the laminate, the microscopic stress distributions exhibit the same patterns as those in the previous study [6]. By contrast, the stress distributions in the vicinity of the free edge (Figs. 5(c) and 6(c)) are markedly different from those of internal area. These microscopic stresses are caused by the mismatch of the deformation between the 0°- and 90°-plies in the vicinity of the free edge, and the peak values of τ_{in} and σ_{22} are 6.97MPa and -12.1MPa, respectively. These results show that it is important to analyze the microscopic stress distribution at interlaminar areas as well as the fiber/matrix interfaces at the free edges of CFRP laminates.

4 Conclusions

In this study, the distributions of microscopic interlaminar stress at a free edge of a cross-ply CFRP laminate subjected to an in-plane on-axis tensile load were analyzed three-dimensionally using the newly proposed method based on the homogenization theory. In the present method, a semiunit cell and the substructure method were employed for the reduction of computational costs. From the analysis results, it is shown that microscopic interlaminar shear stress considerably occurs in the vicinity of the free edge, and such shear stress may cause microscopic failure of laminates. It is therefore important to investigate the microscopic stress distribution at interlaminar areas as well as the fiber/matrix interfaces in the vicinity of free edges.

In addition, it is known that cross-ply CFRP laminates subjected to an off-axis load exhibit complex shear stress distribution at interlaminar areas, due to the rotation of fibers. Thus, the microscopic interlaminar stress analysis under off-axis loading remains for future investigation.

References

[1] K. Goto and T. Matsuda, “Analysis of three-dimensional microscopic stress distributions at a free edge of a unidirectional CFRP laminate”. *Proc. the Conf. on Computational Engineering and Science*, Japan, Vol. 15, No. 2, pp. 679-682, 2010.

[2] E. Sanchez-Palencia, “Non-homogeneous media and vibration theory, Lecture Notes in Physics, No. 127”, *Springer-Verlag*, 1980.

[3] N. Ohno, X. Wu and T. Matsuda “Homogenized properties of elastic-viscoplastic composites with periodic internal structures”. *Int. J. Mech. Sci.*, Vol. 42, pp. 1519-1536, 2000.

[4] T. Matsuda, N. Ohno, H. Tanaka and T. Shimizu “Homogenized in-plane elastic-viscoplastic behavior of long fiber-reinforced laminates”. *JSME Int. J., Ser. A*, Vol. 45, pp. 538-544, 2002.

[5] T. Matsuda, N. Ohno, H. Tanaka and T. Shimizu “Effects of fiber distribution on elastic-viscoplastic behavior of long fiber-reinforced laminates”. *Int. J. Mech. Sci.*, Vol. 45, pp. 1538-1598, 2003.

[6] T. Matsuda, D. Okumura, N. Ohno and M. Kawai “Three-dimensional microscopic interlaminar analysis of cross-ply laminates based on a homogenization theory”. *Int. J. Solids Struct.*, Vol. 44, pp. 8274-8284, 2007.

[7] N.J. Pagano and E.F. Rybicki “On the significance of effective modulus solutions for fibrous composites”. *J. Compos. Meter.*, Vol. 8, pp. 214-228, 1974.

[8] P. Raghavan and S. Ghosh “Concurrent multi-scale analysis of elastic composites by a multi-level computational model”. *Comput. Methods Appl. Mech. Eng.*, Vol. 193, pp. 497-538, 2004.

[9] O.C. Zienkiewicz and R.L. Taylor “The finite element method (5th edn.)”. *Butterworth-Heinemann*, 2000.

[10] N. Ohno, T. Matsuda and X. Wu “A homogenization theory for elastic viscoplastic composites with point symmetry of internal distributions”. *Int. J. Solids Struct.*, Vol. 38, pp. 2867-2878, 2001.

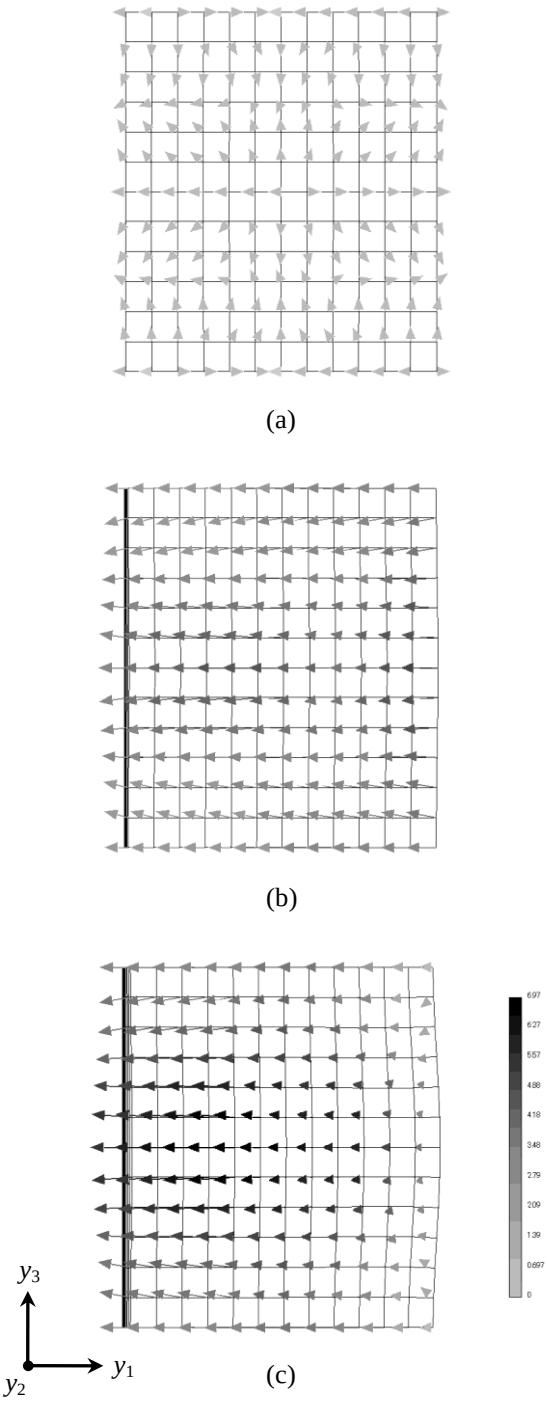

Fig. 5. Distributions of resultant shear stress τ_{in} at the interface of (a)A_1-B_1, (b) A_7-B_7 and (c) A_8-B_8.

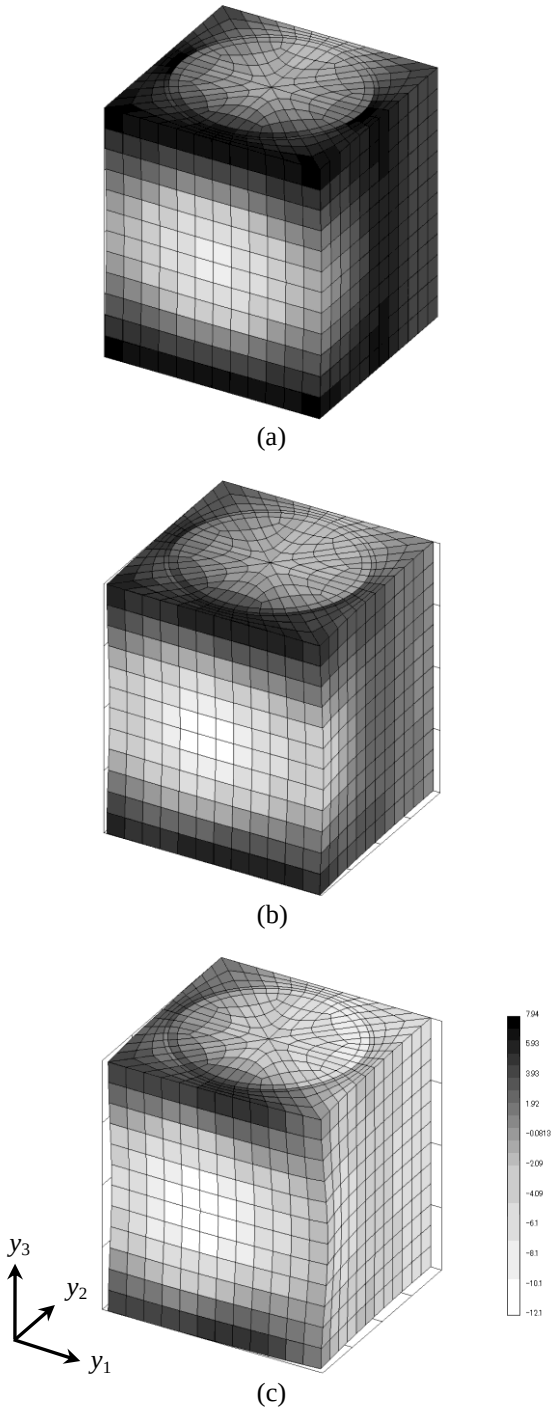

Fig. 6. Distributions of normal stress σ_{22} at the interface of (a)A_1-B_1, (b) A_7-B_7 and (c) A_8-B_8.